Journal of Medicinal Chemistry Article

J. Med. Chem. **2011,** *54,* 939–948 **939**
DOI: 10.1021/jm101110w

Development and Evaluation of Endothelin-A Receptor (Radio)Ligands for Positron Emission Tomography

Kristin Michel,*[,†] Katrin Büther,[†] Marilyn P. Law,[‡,§] Stefan Wagner,[†] Otmar Schober,[†] Sven Hermann,[‡] Michael Schäfers,[‡,§] Burkhard Riemann,[†] Carsten Höltke,[∥,⊥] and Klaus Kopka[†,§,⊥]

[†]*Department of Nuclear Medicine, University Hospital Münster, Albert-Schweitzer-Strasse 33, D-48149 Münster, Germany,* [‡]*European Institute for Molecular Imaging, University of Münster, Mendelstrasse 11, D-48149 Münster, Germany,* [§]*Interdisciplinary Centre of Clinical Research (IZKF), Münster, Germany, and* [∥]*Department of Clinical Radiology, University Hospital Münster, Albert-Schweitzer-Strasse 33, D-48149 Münster, Germany.* [⊥]*Both authors contributed equally to this work and share the senior authorship.*

Received August 26, 2010

The expression and function of endothelin (ET) receptors are abnormal in cardiovascular diseases, tumor progression, and tumor metastasis. A previously reported promising radioligand for positron emission tomography (PET) based on the non-peptide ET_A receptor antagonist PD 156707 showed specific binding to target receptors in the myocardium but high accumulation in bile and intestine, probably because of its high lipophilicity. In this study we describe the synthesis of a series of fluorinated derivatives with hydrophilic building blocks. All compounds were evaluated as high affinity ET_A receptor ligands (**16**, **17**, **23**−**26**, K_i = 1.4−7.9 nM) with high subtype selectivity over the ET_B receptor. [^{18}F]3-Benzo[1,3]dioxol-5-yl-4-{3-[1-(2-{2-[2-(2-fluoroethoxy)ethoxy]ethoxy}ethyl)-1*H*-[1,2,3]triazol-4-ylmethoxy]-4,5-dimethoxybenzyl}-5-hydroxy-5-(4-methoxyphenyl)-5*H*-furan-2-one ([^{18}F]**17**) was synthesized as one of the radioligands of this series that possesses a higher hydrophilicity and an excellent stability in human serum. Improved clearance properties and specific uptake in target organs have been confirmed by biodistribution studies and small animal PET imaging.

Introduction

The endothelin (ET[a]) system comprises a family of three small (21 amino acid) peptides (ET-1, ET-2, and ET-3) and two G-protein-coupled receptor subtypes (ET_A and ET_B). The endothelin receptor subtypes differ with regard to their location and function. While ET_A receptors are primarily located on vascular smooth muscle cells and are responsible for vasoconstriction and cell proliferation, ET_B receptors are located on smooth muscle cells and vascular endothelial cells, causing vasodilation, and are responsible for the clearance of ET-1 from plasma, e.g., in lung tissue.[1] The endothelins and their receptors play an important role in the pathophysiology of cardiovascular, inflammatory, and renal diseases[2−8] and of certain human cancer types.[9−12] In several human malignancies an increased expression of ET-1 has been found.[13−17] The ET_A receptor, the most important ET-1 binding receptor, mediates tumorigenesis and tumor progression by activation of tumor proliferation,[14] invasion,[18] angiogenesis,[19] and inhibition of apoptosis.[20,21] Accordingly, increased ET_A receptor expression has been demonstrated in various cancers.[14,15,22] Because of these findings, the ET_A receptor has been suggested as a target for anticancer therapy. The orally bioavailable ET_A receptor antagonist (2*R*,3*R*,4*S*)-4-(1,3-benzodioxol-5-yl)-1-[2-(dibutylamino)-2-oxoethyl]-2-(4-methoxyphenyl)pyrrolidine-3-carboxylic acid (atrasentan, ABT-627)[23] has been shown to inhibit the growth of ovarian and cervix carcinoma cell xenografts[24,25] and to be effective in patients with advanced androgen-refractory prostate carcinoma.[26,27] The in vivo visualization of the ET system in affected tissue with scintigraphic techniques, such as positron emission tomography (PET), would be highly valuable for clinical diagnosis and evaluation of therapy. Different ET receptor ligands have been developed, radiolabeled by [^{11}C]methylation or [^{18}F]fluorination, and utilized for PET imaging of the ET receptor distribution in a baboon,[28] dog,[29] and rats.[30] However, up to now, none of these approaches have been applied to in vivo imaging of ET receptors in humans. Therefore, there is still a strong motivation to design ET receptor radioligands for clinical applications.

We have focused our investigations on different labeling strategies using the lead structure **1** (PD 156707)[31] (Figure 1), a non-peptide ET_A receptor antagonist with high ET receptor affinity and selectivity.[32,33] We have developed a fluorescent photoprobe, based on the lead structure **1**,[34] and recently published the synthesis of the ^{18}F-labeled derivative [^{18}F]**6** (Scheme 1).[35] The synthesis was achieved by condensation of benzaldehyde **2** with keto ester **3** to afford the bromoethoxy substituted butenolide derivative **4** (Scheme 1). Bromo substitution with silver tosylate (AgOTos) led to the radiolabeling

*To whom correspondence should be addressed. Phone: +49 251 8344701. Fax: +49 251 8347363. E-mail: kristin.michel@uni-muenster.de..

[a] Abbreviations: AcOH, acetic acid; AgOTos, silver tosylate; CH, cyclohexane; clogD, calculated logarithm of distribution coefficient between octanol and water; CT, computer tomography, DMF, dimethylformamide; EA, ethyl acetate; EOS, end of synthesis; ET, endothelin; $ET_{A/B}$, endothelin type A/B; LV, left ventricle; MeOH, methanol; PET, positron emission tomography; PBS, phosphate buffered saline; PEG, polyethylene glycol; SD, standard deviation; SEM, standard error of the mean; TBAF, tetrabutylammonium fluoride; TFA, trifluoroacetic acid; VOIs, volumes of interest.

Published on Web 01/28/2011

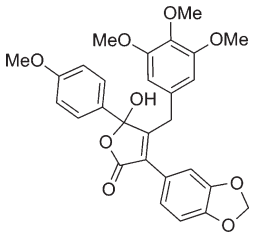

1 (PD 156707)

Figure 1. Structure of lead compound **1**.

Scheme 1. Development of ^{18}F-Labeled ET_A Receptor Radioligand [^{18}F]**6**[a]

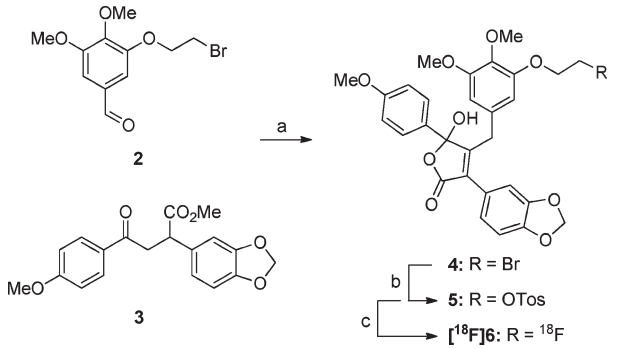

[a] Reaction conditions: (a) (1) Na, MeOH, reflux, 19 h; (2) acetic acid (AcOH), reflux, 7 h; (b) AgOTos, CH_3CN, reflux, 17 h; (c) [^{18}F]fluoride (potassium 222 cryptate), CH_3CN, 85 °C, 10 min.

precursor **5**, which was converted to the ^{18}F-substituted target compound [^{18}F]**6** using the [^{18}F]fluoride (potassium-222 cryptate) system.

The ET_A receptor radioligand [^{18}F]**6** was applied to first in vivo studies. The myocardium of wild-type mice, normally showing a high ET_A receptor density (78.5 ± 8.3 amol·mm^{-2}),[36] was successfully visualized by PET. Specific uptake in the myocardium was confirmed in biodistribution studies by predosing experiments using compound **1**. Unfortunately, the radioligand [^{18}F]**6** revealed an insufficient metabolic stability and a high degree of accumulation in liver, intestine, and bile, presumably because of its high lipophilicity.

One approach to modify pharmacokinetic properties is to attach polyethylene glycol (PEG) units, which are known to have significant effects on pharmacokinetic and pharmacodynamic properties of peptides and small-molecule drugs.[37,38] Moreover, PEG conjugates increase solubility in aqueous media either by permanent PEGylation or in cleavable prodrug approaches.[39]

1,2,3-Triazoles possess a large dipole moment and act as weak hydrogen bond acceptors and may therefore be regarded as hydrophilic building blocks.[40] Additionally, they show high stability against oxidation or reduction and may contribute to receptor binding because of stacking interactions and hydrogen bonding.[41]

In this study we describe the synthesis and in vitro characterization of a new series of selective ET_A receptor ligands and their labeling precursors derived from the lead structure **1** modified with hydrophilic building blocks to improve their pharmacokinetic properties. We introduced a triazole group, following the concept of click chemistry introduced by Sharpless et al.,[42] and a PEG spacer, which was known by our previous results to have neither effect on receptor affinity nor subtype selectivity.[34] A first candidate was radiolabeled by nucleophilic substitution of a tosylate bearing synthon by [^{18}F]fluoride in a semiautomatic one-pot two-step procedure. The [^{18}F]ET_A receptor ligand was applied to biodistribution studies and small animal PET imaging for evaluation of uptake and clearance properties in vivo.

Results and Discussion

Chemistry. Our aim was to synthesize triazole and PEG containing derivatives of **1**. We started with the synthesis of the azido and propargyl bearing benzaldehydes **10a**−**c** and the fluorinated aldehyde **10d**. The compounds were prepared in 68−97% yield by reaction of commercially available 4, 5-dimethoxy-3-hydroxybenzaldehyde and propargyl bromide, mesylated or tosylated PEG derivatives **7**−**9** under basic conditions in dimethylformamide (DMF) (Scheme 2). 1, 3-Dipolar cycloaddition of propargyl substituted benzaldehyde **10a** and azido-substituted PEG derivative **11** was carried out using copper(II) sulfate and sodium ascorbate in DMF which affords the triazole containing aldehyde **12** in 84% yield. All PEG derivatives (**7**−**9** and **11**) were synthesized following literature procedures.[34,43] The condensation reaction of the aldehydes **10a**−**c** and **12** with keto ester **3** afforded the butenolides **13**−**15** as suitable click precursors in yields of 72−88% and the ET_A receptor ligands **16** and **17** as nonradioactive target compounds in yields of 27% and 63% (Scheme 2). The alkyne- and azido-substituted butenolides **13**−**15** can be used for the synthesis of the ^{19}F-reference compounds and as precursors for radiolabeling in a two-step procedure with the corresponding ^{18}F-labeled synthons.

With the alkyne- and azido-substituted butenolide derivatives **14** and **15** in hand, we prepared a new series of fluorinated, triazole, and PEG containing compounds of the lead structure **1** by 1,3-dipolar cycloaddition. ET_A receptor ligands **19** and **23**−**26** were synthesized in yields of 28−61% in analogy to the procedure described for **12** (Scheme 2) by click reaction with fluoropyridyl derivatives **18** and **20**, sulfonamides **21a** and **21b**, and propargyl fluoride (**22**) (Scheme 3).

Receptor Binding Studies. Compounds **16**, **17**, **19**, and **23**−**26** were subjected to receptor binding studies. The binding potencies toward endothelin receptors were determined by competition binding studies using [^{125}I]ET-1 and mouse membrane preparations of myocardial ventricles. The binding of the nonselective ET receptor ligand [^{125}I]ET-1 to ventricular membranes was specific, saturable and of high affinity. The inhibition constants $K_i(ET_A)$ and $K_i(ET_B)$ are displayed in Table 1. All newly prepared butenolide derivatives show a high affinity to the ET_A receptor with K_i values ranging from 1.4 to 7.9 nM and are comparable to our previously reported derivative **6** with K_i value of 1.1 nM. All compounds exhibit higher affinities to the ET_A receptor than to the ET_B receptor with ratios for $K_i(ET_B)/K_i(ET_A)$ from ~11 for compound **23** to ~3500 for compound **16**. This wide tolerance for different substituents is consistent with the detailed structure−activity relationship determined by Patt et al.[33] However, the selectivities of the ligands suffer from these modifications. Ligand **17** displays the best selectivity (3521:1) to the ET_A receptor combined with a clogD value of 1.79 which makes it a rather hydrophilic compound along with **19** with a clogD value of 1.50 (Table 1). For this reason, we chose **17** as the first candidate for the development of its radiofluorinated component [^{18}F]**17** and for the first in vitro and in vivo studies.

Scheme 2. Synthesis of Butenolide Derivatives **13**−**17**[a]

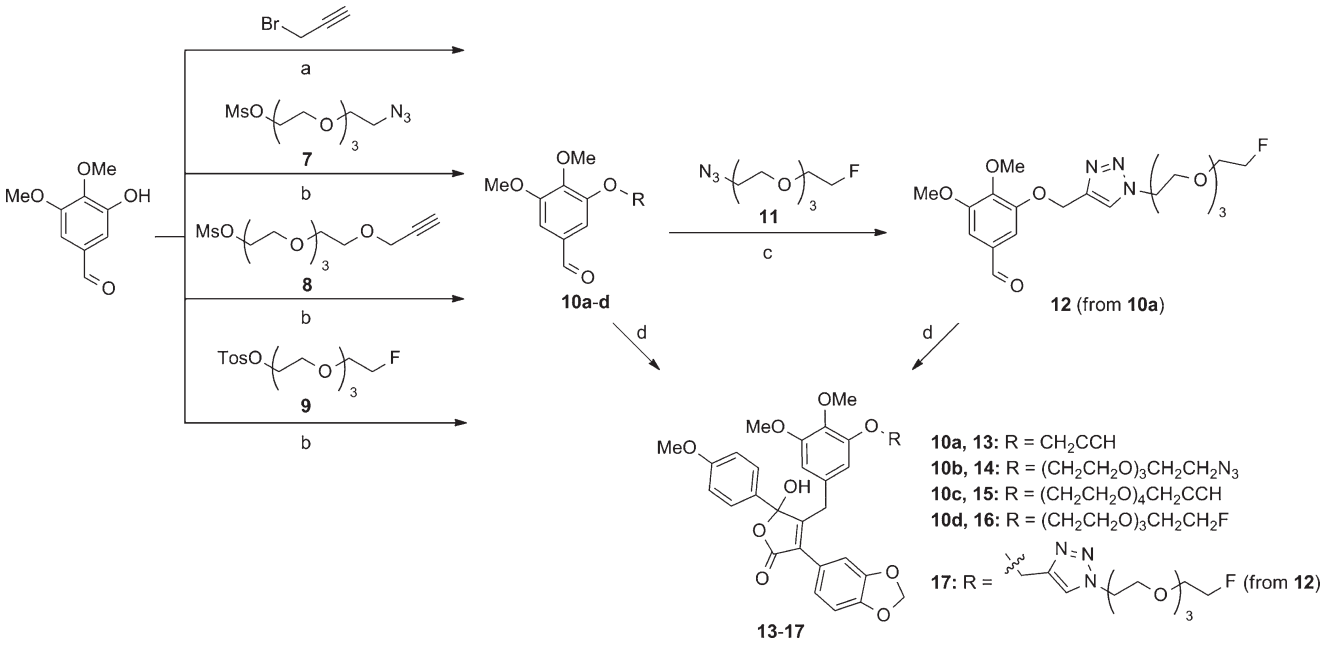

[a] Reaction conditions: (a) K_2CO_3, DMF, 80 °C, 2 h; (b) Cs_2CO_3, DMF, 90 °C, 1.5 h; (c) $CuSO_4 \cdot 5H_2O$, sodium ascorbate, DMF, room temp, 12 h; (d) (1) **3**, Na, MeOH, reflux, 19 h; (2) AcOH, reflux, 7 h.

Scheme 3. Synthesis of 1,2,3-Triazoles **19** and **23**−**26**[a]

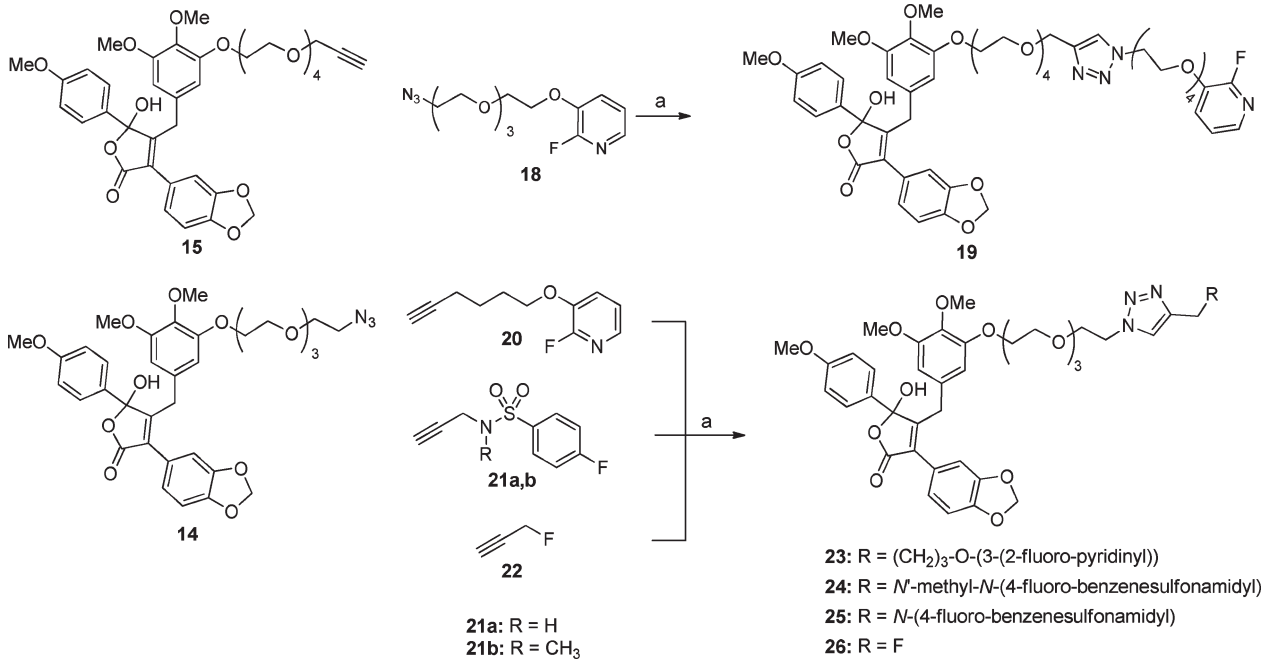

[a] Reaction conditions: (a) $CuSO_4 \cdot 5H_2O$, sodium ascorbate, DMF, room temp, 12 h.

Radiochemistry. We first attempted a one-step radiofluorination procedure with typical reaction conditions for fluorine-to-tosyloxy substitution (data not presented). In spite of using different solvents at different temperatures and varying reaction times, we observed very low radiochemical yields (< 5%) and many radioactive side products. So we changed our labeling strategy to the 1,3-dipolar azide−alkyne cycloaddition following the concept of click chemistry introduced by Sharpless et al.,[42] which has also been used for ^{18}F-radiolabeling methods, in order to take advantage of its selectivity, reliability, and speed under mild aqueous Cu^I-promoted reaction conditions.[44−50] For the radiosynthesis of [^{18}F]**17** we developed a one-pot two-step procedure avoiding the time-consuming isolation of the intermediate radiosynthon [^{18}F]**11** by semipreparative HPLC. As the first step, the precursor tosylate **27** was radiofluorinated in DMF at 120 °C using [^{18}F]tetra-*n*-butylammonium fluoride ([^{18}F]TBAF) in a reaction time of 10 min. Subsequently the precursor **13**, dissolved in 200 μL of DMF, and aqueous solutions of copper(II) sulfate pentahydrate and sodium ascorbate were added at 60 °C (Scheme 4). This approach successfully provided the 1,2,3-triazole-linked PEG-ET$_A$

Table 1. Inhibition Constants of the Fluorinated Target Compounds Obtained via Radioligand Binding Assay Using Mouse Ventricular Membrane Preparations and the Calculated log *D* Values of the Tautomeric Butenolids **A** and **B** in Comparison with Experimentally Determined log *D* Values

	K_i [a] ± SEM (nM)			log *D*		
compound	ET_A	ET_B	ET_B/ET_A	clogD [b] (**A**)	clogD [b] (**B**)	log *D* (exptl) [c]
6	1.1 ± 0.6	240 ± 16	218	3.51	2.36	1.71 ± 0.05
16	1.4 ± 0.7	418 ± 213	299	2.40	1.25	
17	2.4 ± 0.7	8450 ± 4555	3521	1.79	0.64	0.89 ± 0.09
19	4.4 ± 2.1	5340 ± 2292	1214	1.50	0.35	
23	3.5 ± 2.4	37 ± 22	11	3.90	2.75	
24	3.9 ± 1.2	288 ± 145	74	3.26	2.11	
25	7.3 ± 3.6	893 ± 566	122	2.77	1.62	
26	7.9 ± 1.7	6450 ± 6120	816	2.16	1.01	

[a] Values are the mean ± SEM of three experiments. [b] clogD values were calculated for the closed form **A** and the keto carboxylate **B** by ACD/Chemsketch, version ACD/Labs 6.00 (log *D* = log *P* at physiological pH (7.4)). [c] log *D* values were determined for compounds [^{18}F]**17** and [^{18}F]**6**; values are the mean ± range of two independent experiments.

Scheme 4. Radiosynthesis of ^{18}F-Labeled [^{18}F]**17**[a]

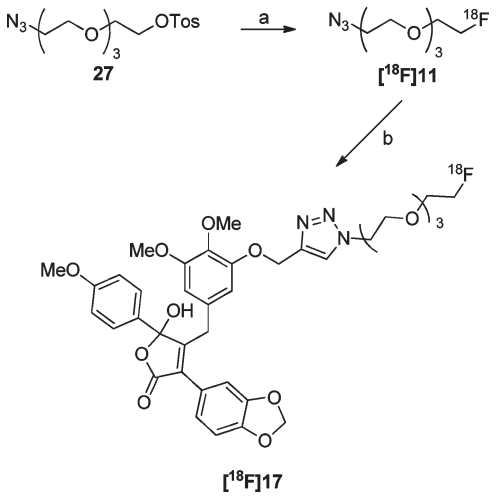

[a] Reaction conditions: (a) [^{18}F]TBAF, DMF, 120 °C, 10 min; (b) **13**, $CuSO_4 \cdot 5H_2O$, sodium ascorbate, DMF, 60 °C, 10 min.

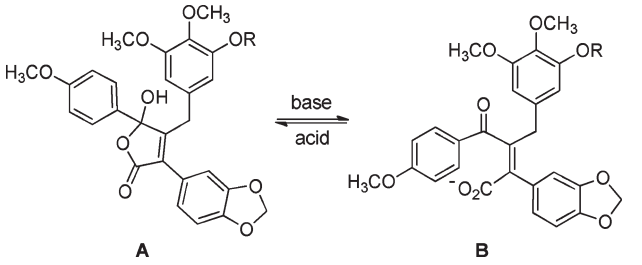

Figure 2. Butenolide tautomerization between closed form A and keto carboxylate B.

receptor ligand [^{18}F]**17** with a radiochemical yield of 24 ± 9% (decay corrected, $n = 3$) in 130 min from the end of radionuclide production including isolation by semipreparative HPLC and formulation. The radioligand was formulated in phosphate buffered saline (PBS) to determine log $D_{7.4}$ values and to study its in vitro stability in human serum at 37 °C. The radiochemical purity of the radioligand [^{18}F]**17** was >98%, and the specific activity was 17−35 GBq·μmol^{-1} at the end of synthesis (EOS). Further optimization of the radiochemical yield as well as the minimization of the reaction and purification time would be necessary for clinical use considering the short half-life of fluorine-18 (110 min) and will be accomplished if the in vivo performance of the tracer in disease models with up-regulated ET_A receptor expression appears promising.

Hydrophilicity. As a marker of hydrophilicity, the partition coefficients (log *D* values) of [^{18}F]**17** and [^{18}F]**6** were determined experimentally to be 0.89 ± 0.09 and 1.71 ± 0.05 (mean ± SD). However, calculated $clogD_{7.4}$ values obtained by the software ACD/Chemsketch (version ACD/Labs 6.00) revealed values of 1.79 for **17** and 3.51 for **6**. The significant difference between calculated and experimental values could be partially an effect of the tautomerism that occurs under physiological pH conditions which was discovered and examined with NMR by Patt et al. (Figure 2).[33] The ketocarboxylates **B** are more hydrophilic than the closed forms **A** ($\Delta clogD_{7.4} = 1.15$, Table 1) and have a decreasing effect on the experimental log *D* value which was determined in PBS buffer at a pH value of 7.4. The deviation of experimentally determined and calculated log *D* values depends on the equilibrium of the two tautomers and is significantly lower for the open butenolide derivative **B**.

The influence of the modifications with the hydrophilic building blocks PEG and triazole is displayed by the calculated log *D* values in Table 1. Compared to the fluoroethoxy substituted butenolide **6**, the PEGylated derivative **16** reveals a significant shift of 1.11 clogD units which displays an increase in the hydrophilicity of 13 times. Modification with a triazole leads to an additional difference of 0.60 for compound **17** and 0.24 for the ligand **26**, indicating a 2−4 times increase of hydrophilicity. The introduction of less hydrophilic labeling synthons like 4-fluorobenzenesulfonamides reduces the effects displayed by the clogD values of compound **25** (clogD(**A**) = 2.76) and the N-methylated derivative **24** (clogD(**A**) = 3.27). The use of an alkyl chain containing synthon in the ligand **23** actually fully compensates the hydrophilic effects of the PEG and triazole moieties. When the alkyl spacer between the 2-fluoropyridinyl substituent and the triazole ring was replaced by an additional PEG unit, the most hydrophilic derivative **19** (clogD(**A**) = 1.50) of this series of ET_A-receptor ligands was obtained.

Metabolic Stability. Metabolic studies of fluoroethoxy derivative [^{18}F]**6** were carried out in vitro by incubation with rat plasma and in vivo with blood samples taken at several time points after tail vein injection. These studies revealed polar radiometabolites within 20 min after injection in mice.[35] A possible metabolic pathway could be the defluoroethylation which leads to 2-[^{18}F]fluoroethanol and its oxidation products [^{18}F]fluoroacetaldehyde and [^{18}F]fluoroacetate, which were also observed by Zoghbi et al. for a radiofluorinated dopamine transporter ligand.[51] This problem of defluoroethylation should be circumvented by the introduction of

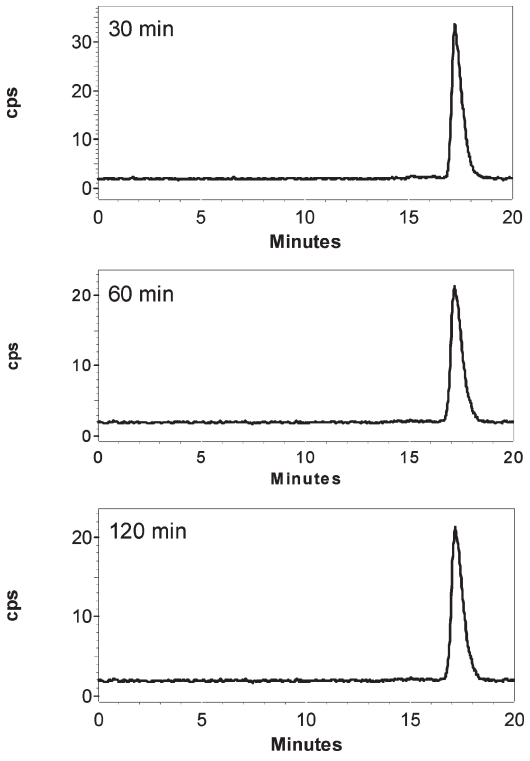

Figure 3. Stability of [^{18}F]**17** (t_R = 17.2 min; C18, linear gradient from 40% to 95% CH_3CN in water (0.1% TFA) over 5 min following 95% CH_3CN (0.1% TFA) in water (0.1% TFA) over 15 min, 1.5 mL·min^{-1}) after incubation in human serum in vitro at 37 °C after 30 min (top), 90 min (middle), and 120 min (bottom).

the PEG spacer and the triazole moiety as well as the choice of different binding modes of the fluorine atom (aliphatic, aromatic, and heteroaromatic).

Preliminary metabolic studies of [^{18}F]**17** were carried out by in vitro incubation of human serum at 37 °C where an excellent stability was observed. Even after long-term incubation for up to 120 min, only parent [^{18}F]**17** and no radiometabolites were detected by radio-HPLC (Figure 3).

Ex Vivo Biodistribution Studies. Figure 4 shows the biodistribution of [^{18}F]**17** and the effects of predosing with unlabeled ET_A receptor antagonist **1** on tissue uptake of radioactivity at 30 min after injection. There was uptake of radioactivity in duodenum and stomach in control mice (predosing with water), uptake indices being significantly greater than that for plasma. In other tissues, however, uptake indices were comparable to (myocardium, liver, kidney, lung, colon) or lower than (spleen, muscle, brain) plasma. Predosing with compound **1** significantly reduced the uptake in myocardium, kidney, lung, and liver, indicating that the uptake of [^{18}F]**17** is low but specific.

There was considerable radioactivity in the contents of the stomach and duodenum and in bile and urine (data not shown). When the gall bladder was visible (nine mice), high levels of radioactivity were detected in the bile (uptake index 8−67), and no significant difference between predosing with water or receptor ligand **1** was observed. Urine samples were obtained from four mice with moderate levels of radioactivity detected (uptake index 11−18).

In Vivo PET Studies. For PET studies mice were intravenously injected with the radiotracer [^{18}F]**17** with its biodistribution monitored for 90 min by dynamic PET scanning, co-registered to a CT. Figure 5 shows coronal whole body

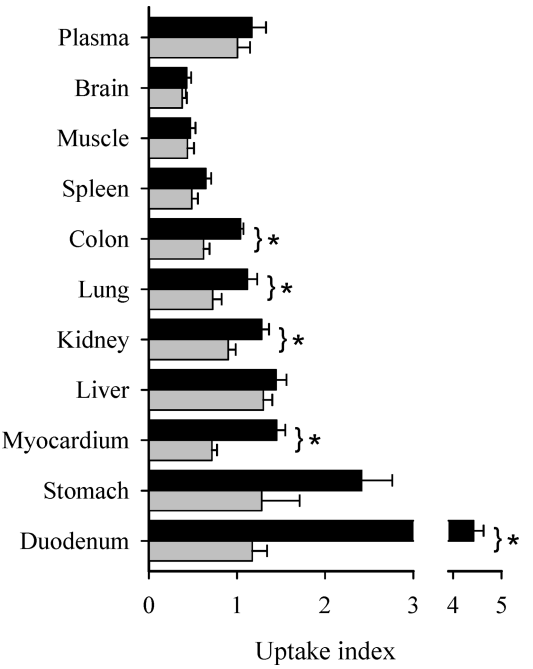

Figure 4. Effect of the ET_A receptor antagonist **1** on radioactivity in tissues of mice at 30 min after intravenous injection of [^{18}F]**17**. Water for injection (5 mice) or compound **1** at 5 μmol·kg^{-1} (six mice) was injected 10 min before [^{18}F]**17** at 2.5 nmol·kg^{-1}. Tissue radioactivity (mean uptake index with standard errors) is shown for each tissue: (*) significant difference (t test, $p < 0.05$); (black bar) water for injection; (gray bar) compound **1**.

images at four different time frames and a co-registration to the CT. Low tracer uptake of nontarget organs such as brain, lung, and muscle was observed. There was initial high uptake in the liver followed by rapid clearance into the gallbladder and the gastrointestinal tract. There was also notable uptake in the bladder indicative of renal excretion. The low accumulation of activity in the skeleton suggests that the extent of tracer defluorination and formation of free [^{18}F]fluoride is negligible.

Figure 6 shows time activity curves for volumes of interest (VOIs) in the blood, myocardium, and lung. The curves do not demonstrate a significant retention of [^{18}F]**17** in myocardium and lung. The nanomolar carrier amount of **17** injected, however, may be too high to enable the detection of specific uptake by small animal PET in vivo.

Figure 7 shows early uptake of radioactivity in liver with subsequent clearance. The uptake and clearance of radioactivity in the gall bladder (bile) were slightly later than in the liver. The kidney curve shows an early increase and a subsequent loss of radioactivity which was associated with an increase in radioactivity in the bladder (urine).

In comparison to compound [^{18}F]**6**, the more hydrophilic compound [^{18}F]**17** shows improved pharmacokinetic properties. Whereas high accumulation in liver and kidney and no activity in the bladder were observed for [^{18}F]**6**, [^{18}F]**17** shows rapid clearance from the liver and accumulation of the tracer in the bladder. This is clearly a shift toward improved properties for in vivo imaging especially of organs in the abdomen.

Conclusion

We here report the synthesis of a series of new high affinity ET_A selective receptor ligands with clogD values ranging from

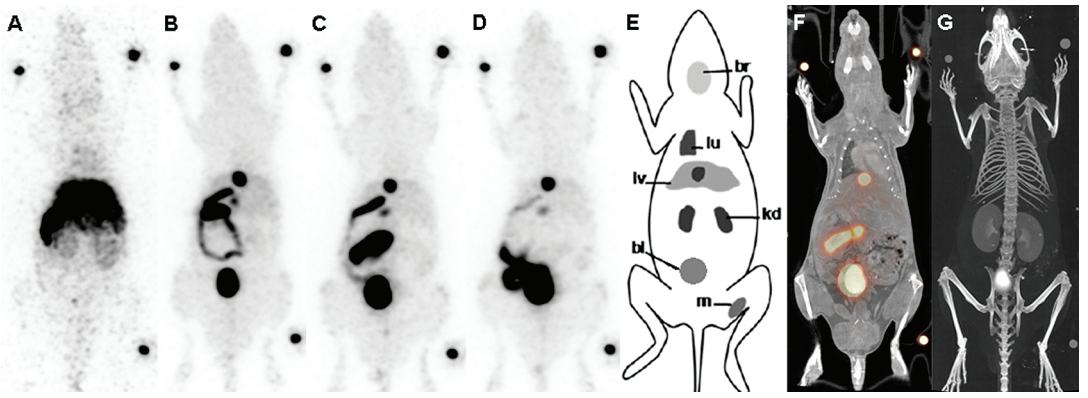

Figure 5. Biodistribution in small-animal PET and PET/CT after intravenous injection of [^{18}F]**17** in a Balb/c mouse. Panels A−D display maximum intensity projections of the radioactivity in the time frames 2−3 min (A), 15−20 min (B), 50−60 min (C), 90−110 min (D). Additionally an overview over the regions of interest (E), a fused PET/CT image (F), and a CT image (E) of the mouse are shown.

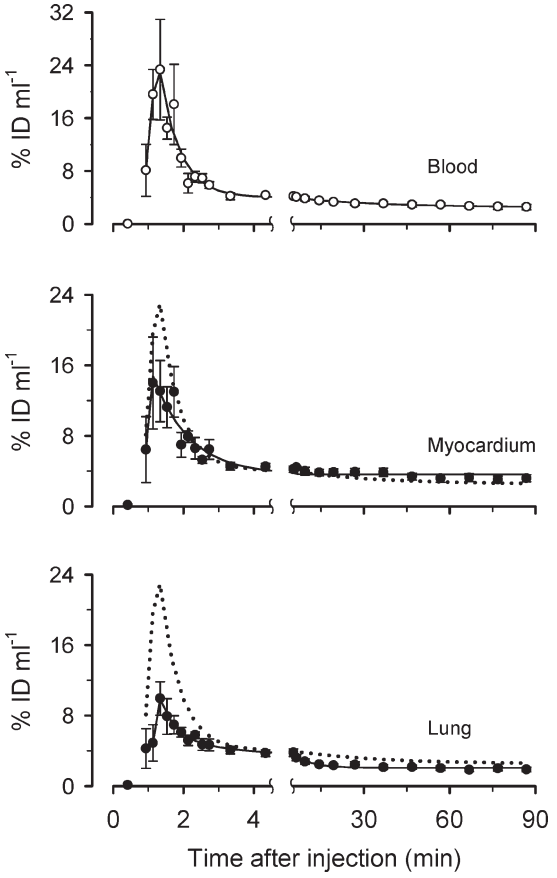

Figure 6. Uptake and clearance of radioactivity in tissues of mice after intravenous injection of [^{18}F]**17** (5−10 MBq, 13−26 nmol·kg^{-1}) assessed by small animal PET. CT guided volumes of interest (VOIs) were drawn in selected tissues and time activity curves computed. Symbols at each time point indicate mean values for four mice with standard errors. Unbroken lines indicate empirical fits to the mean values. Dotted lines show the fit for blood (VOIs in left ventricle) shown in the upper panel. Note the break in the time axis.

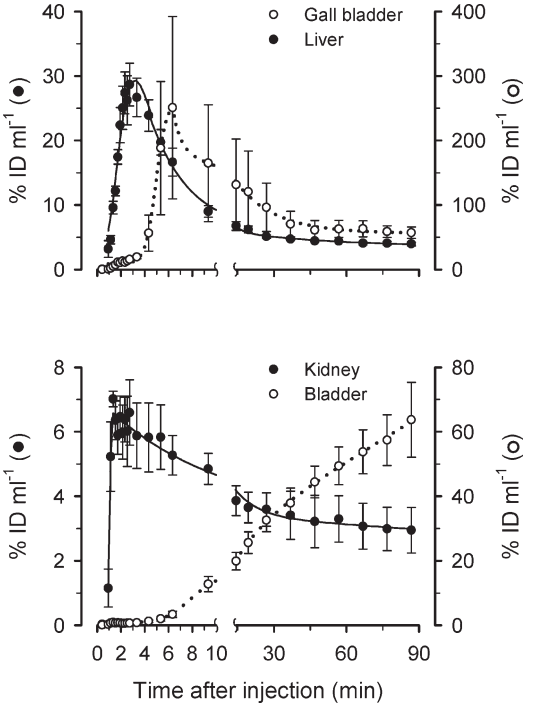

Figure 7. Uptake and clearance of radioactivity in organs, usually involved in metabolism of radiotracers, after intravenous injection of [^{18}F]**17** (5−10 MBq, 15−25 nmol·kg^{-1}) into mice assessed by small animal PET. CT guided regions of interest were drawn in liver, gall bladder, kidney (cortex/medulla), and urinary bladder and time activity curves computed. Symbols at each time point indicate mean values for four mice with standard errors. Lines indicate empirical fits to the mean. Upper panel: left axis shows scale for liver, and right shows scale for gall bladder. Lower panel: left axis shows scale for kidney, and right shows scale for urinary bladder. Note the break in the time axis.

1.50 to 3.90 which allow systematic investigations of pharmacokinetic properties and metabolic stability. The first candidate has been successfully radiolabeled by a semiautomatic one-pot two-step procedure using the concept of click chemistry. The radioligand [^{18}F]**17** revealed a lower log *P* value compared to compound [^{18}F]**6** described earlier by our group[35] and showed a high serum stability. In vivo biodistribution studies confirmed favorable clearance properties due to a mixture of hepatobiliary and renal excretion pathways. Additionally, a specific tracer uptake in myocardium, lung, colon, kidney, and duodenum (organs with significant ET_A expression) was demonstrated by predosing experiments. In summary, the class of [^{18}F]**17** analogs represents potential radiotracers for investigating endothelin receptors in vivo. In the next step, the ^{18}F-radiosyntheses of compounds **16**, **19**, and **23**−**26** will be developed and preclinical PET/CT studies in disease models with up-regulated ET_A receptor expression will be assessed.

Experimental Section

General. All reagents and solvents were purchased from commercial sources and used without further purification unless otherwise specified. Melting points (mp) are uncorrected and were determined in capillary tubes on a Stuart Scientific SMP3 capillary melting point apparatus. ^{1}H, ^{13}C, and ^{19}F NMR spectra were recorded on Bruker AV400 or AV300 spectrometers. Tetramethylsilane (^{1}H), $CDCl_3$ (^{13}C), and $CFCl_3$ (^{19}F) were used as internal references, and all chemical shift values were recorded in ppm (δ). Mass spectrometry analysis (ESI-EM) was performed using a MicroTof (Bruker Daltronics, Bremen) instrument. The mass calibration was carried out before the measurement using sodium formate clusters. Thin layer chromatography (TLC) was carried out on silica gel coated polyester backed TLC plates (Polygram, SIL G/UV_{254}, Macherey-Nagel) using solvent mixtures of cyclohexane (CH), ethyl acetate (EA), and methanol (MeOH). Compounds were visualized by UV light (254 nm). (Radio)HPLC was performed on the following system: Two pumps and S-2500 UV detector (Herbert Knauer GmbH, Berlin, Germany), GabiStar γ-detector (Raytest Isotopenmessgeräte GmbH, Straubenhardt, Germany). The recorded data were processed by the ChromGate HPLC software (Knauer). Each ^{18}F-labeled compound was identified by retention time (t_R) on the radio-HPLC system and co-injection of the corresponding nonradioactive reference compound. The purity of all biologically tested and radioactive compounds was confirmed by analytical reversed phase RP-HPLC (unless otherwise stated: Nucleosil 100-5 C18, 250 mm × 4.6 mm; flow, 1.5 mL·min^{-1}; 4 min 40% CH_3CN (0.1% TFA) in water (0.1% TFA) following a linear gradient from 40% to 95% CH_3CN in water (0.1% TFA) over 31 min). All final compounds were found to have ≥95% purity unless otherwise specified. Sodium 2-benzo[1,3]dioxol-5-yl-4-(4-methoxyphenyl)-4-oxo-3-(3,4,5-trimethoxybenzyl)but-2-enoate,[32] 2-(1,3-benzodioxol-5-yl)-1-(4-benzyloxyphenyl)-4-oxobutyric acid methyl ester **3**,[32] methanesulfonic acid 2-{2-[2-(2-prop-2-ynyloxyethoxy)-ethoxy]ethoxy}ethyl ester **8**,[43] 1-azido-2-{2-[2-(2-fluoroethoxy)ethoxy]ethoxy}ethane **11**,[43] toluene-4-sulfonic acid 2-{2-[2-(2-azidoethoxy)ethoxy]ethoxy}ethyl ester **27**,[43] 4-fluoro-*N*-methyl-*N*-(prop-2-inyl)benzolsulfonamide **21b**,[52] and 2-fluoro-3-(hex-5-ynyloxy)pyridine **20**[53] were synthesized following literature procedures. Toluene-4-sulfonic acid 2-{2-[2-(2-fluoroethoxy)ethoxy]ethoxy}ethyl ester **9** was synthesized according to the corresponding methanesulfonic acid derivative.[43] The analytical data correspond to literature data.[54] Methanesulfonic acid 2-{2-[2-(2-azidoethoxy)ethoxy]ethoxy}ethyl ester **7**, 3-(2-{2-[2-(2-azidoethoxy)ethoxy]ethoxy}ethoxy)-4,5-dimethoxybenzaldehyde **10b**, and 3-benzo[1,3]dioxol-5-yl-4-(3-(2-{2-[2-(2-azidoethoxy)ethoxy]ethoxy}ethoxy)-4,5-dimethoxybenzyl)-5-hydroxy-5-(4-methoxyphenyl)-5*H*-furan-2-one **14** were synthesized as described previously.[34] 3-(2-{2-[2-(2-Azidoethoxy)ethoxy]-ethoxy}ethoxy)-2-fluoropyridine **18** was synthesized and generously provided by Daniela Schrigten[55] using a procedure similar to that described by Kuhnast et al.[56] All animal experiments were conducted in accordance with local institutional guidelines for the care and use of laboratory animals.

General Procedure: Preparation of 3-Benzo[1,3]dioxol-5-yl-4-aryl-5-hydroxy-5-(4-methoxyphenyl)-5*H*-furan-2-one Derivatives (16, 17). Compounds **16** and **17** were synthesized from 2-(1,3-benzodioxol-5-yl)-1-(4-benzyloxyphenyl)-4-oxobutyric acid methyl ester **3** (3.7−16.0 mmol, 1 equiv), the corresponding benzaldehydes **10d** and **12** (1.04 equiv), and sodium metal (1.04 equiv) in methanol (2.5 mL·mmol^{-1}) followed by reaction with acetic acid (2.5 mL·mmol^{-1}) according to the method described by Doherty et al.[32] The crude products were purified by column chromatography.

3-Benzo[1,3]dioxol-5-yl-4-{3-(2-(2-(2-(2-fluoroethoxy)ethoxy)-ethoxy)ethoxy)-4,5-dimethoxybenzyl}-5-hydroxy-5-(4-methoxyphenyl)-5*H*-furan-2-one (16). 16 was obtained from **10d** (1.3 g, 3.5 mmol) and **3** (1.2 g, 3.6 mmol) as a viscous, yellow oil (1.4 g, 2.2 mmol, 63%). TLC (CH/EA, 1:1): R_f = 0.13. ^{1}H NMR (300 MHz, $CDCl_3$) δ 7.39 (d, ^{3}J = 7.3 Hz, 2H), 6.97−6.92 (m, 2H), 6.88−6.78 (m, 3H), 6.19 (s, 1H), 6.02 (s, 1H), 5.96 (s, 2H), 4.97 (br, 1H), 4.63−4.59 (m, 1H), 4.47−4.43 (m, 1H), 4.01−3.95 (m, 2H), 3.79 (s, 3H), 3.79−3.75 (m, 2H), 3.74 (s, 3H), 3.72−3.61 (m, 12H), 3.63 (s, 3H). ^{13}C NMR (75 MHz, $CDCl_3$) δ 171.0, 160.3, 160.2, 153.0, 152.2, 148.1, 147.7, 137.2, 131.8, 128.9, 128.2, 127.4, 123.1, 123.0, 113.9, 109.4, 108.4, 108.1, 106.2, 105.7, 101.3, 83.1 (d, ^{1}J = 168 Hz), 70.7, 70.6, 70.6, 70.5, 70.3 (d, ^{2}J = 20 Hz), 69.8, 68.6, 60.8, 55.9, 55.3, 32.0. ^{19}F NMR (282 MHz, $CDCl_3$,) δ −222.7. MS-ES-EM m/z = 693.2319 [(M + Na)$^+$], calcd for $C_{35}H_{39}FO_{12}$Na 693.2318. HPLC t_R = 19.01 min (95.1%).

3-Benzo[1,3]dioxol-5-yl-4-{3-[1-(2-{2-[2-(2-fluoroethoxy)ethoxy]-ethoxy}ethyl)-1*H*-1,2,3-triazol-4-ylmethoxy]-4,5-dimethoxybenzyl}-5-hydroxy-5-(4-methoxyphenyl)-5*H*-furan-2-one (17). 17 was obtained from **12** (1.7 g, 3.7 mmol) and **3** (1.2 g, 3.6 mmol) as a viscous, yellow oil (0.7 g, 1.0 mmol, 27%). TLC (CH/EA, 1:8): R_f = 0.20. ^{1}H NMR (300 MHz, $CDCl_3$) δ 7.85 (s, 1H), 7.47−7.39 (m, 2H), 6.93−6.70 (m, 6H), 6.62 (d, ^{4}J = 1.7 Hz, 1H), 6.05 (d, ^{4}J = 1.6 Hz, 1H), 5.93 (s, 2H), 5.13 (s, 2H), 4.64−4.57 (m, 1H), 4.54−4.47 (m, 2H), 4.47−4.43 (m, 1H), 3.82−3.56 (m, 23H). ^{13}C NMR (75 MHz, $CDCl_3$) δ 171.1, 160.6, 160.4, 153.2, 151.2, 148.2, 147.8, 143.6, 137.1, 132.2, 129.2, 128.7, 127.6, 125.1, 123.4, 123.2, 114.0, 109.4, 108.5, 108.3, 106.6, 106.3, 101.4, 83.3 (d, J = 169 Hz), 70.9, 70.6, 70.6, 70.6, 70.4, 69.4, 61.7, 61.0, 56.0, 55.5, 50.7, 32.2. ^{19}F NMR (282 MHz, $CDCl_3$,) δ −222.7. MS-ES-EM m/z = 774.2641 [(M + Na)$^+$] calcd for $C_{38}H_{42}FN_3O_{12}$Na 774.2645. HPLC t_R = 21.23 min (99.5%).

General Procedure: Synthesis of 1,2,3-Triazols 19 and 23−26. Aqueous solutions of copper(II) sulfate pentahydrate (0.4 M, 0.36 mL·mmol^{-1}) and sodium ascorbate (0.6 M, 0.24 mL·mmol^{-1}) were added to an equimolar solution of the azide and the corresponding alkyne compound (0.5−4.5 mmol) in DMF (10 mL·mmol^{-1}). The mixture was stirred at room temperature overnight. The solvent was evaporated in vacuo, and the residue was redissolved in H_2O and $CHCl_3$. The aqueous layer was extracted twice with $CHCl_3$ (5 mL), and the combined organic layers were dried ($MgSO_4$). After evaporation of the solvent, the residue was purified by silica gel column chromatography.

3-Benzo[1,3]dioxol-5-yl-4-[3-(2-{2-[2-(2-{1-[2-(2-{2-[2-(2-fluoropyridin-3-yloxy)ethoxy]ethoxy}ethoxy)-ethyl]-1*H*-1,2,3-triazol-4-ylmethoxy}ethoxy)ethoxy]ethoxy}ethoxy)-4,5-dimethoxybenzyl]-5-hydroxy-5-(4-methoxyphenyl)-5*H*-furan-2-one (19). 19 was obtained from **15** (0.35 g, 0.5 mmol) and **18** (0.16 g, 0.5 mmol) as a yellow oil (250 mg, 0.24 mmol, 49%). TLC (EA/MeOH, 1:3): R_f = 0.30. MS-ES-EM m/z = 1043.3905 [(M + Na)$^+$] calcd for $C_{51}H_{61}FN_4O_{17}$Na 1043.3908. HPLC t_R = 21.47 min (96.0%).

3-Benzo[1,3]dioxol-5-yl-4-[3-(2-{2-[2-(2-{4-[4-(2-fluoropyridin-3-yloxy)butyl]-1,2,3-triazol-1-yl}ethoxy)ethoxy]ethoxy}ethoxy)-4,5-dimethoxybenzyl]-5-hydroxy-5-(4-methoxyphenyl)-5*H*-furan-2-one (23). 23 was obtained from **20** (0.10 g, 0.5 mmol) and **14** (0.35 mg, 0.5 mmol) as a yellow oil (1.7 g, 0.37 mmol, 84%). TLC (EA/MeOH, 15:1): R_f = 0.38. MS-ES-EM m/z = 909.3303 [(M + Na)$^+$] calcd for $C_{46}H_{51}FN_4O_{13}$Na 909.3329. HPLC t_R = 24.18 min (98.6%).

***N*-[1-(2-{2-[2-(2-{5-[4-Benzo[1,3]dioxol-5-yl-2-hydroxy-2-(4-methoxyphenyl)-5-oxo-2,5-dihydrofuran-3-ylmethyl]-2,3-dimethoxyphenoxy}ethoxy)ethoxy]ethoxy}ethyl)-1*H*-1,2,3-triazol-4-ylmethyl]-4-fluoro-*N*-methylbenzenesulfonamide (24). 24** was obtained from **21b** (0.11 g, 0.5 mmol) and **14** (0.35 g, 0.5 mmol) as a yellow oil (0.29 g, 0.30 mmol, 61%). TLC (CH/EA, 1:5): R_f = 0.18. MS-ES-EM m/z = 943.2840 [(M + Na)$^+$] calcd for $C_{45}H_{49}FN_4O_{14}$Na 943.2842. HPLC t_R = 25.35 min (99.1%).

***N*-[1-(2-{2-[2-(2-{5-[4-Benzo[1,3]dioxol-5-yl-2-hydroxy-2-(4-methoxyphenyl)-5-oxo-2,5-dihydrofuran-3-ylmethyl]-2,3-dimethoxyphenoxy}ethoxy)ethoxy]ethoxy}ethyl)-1*H*-1,2,3-triazol-4-ylmethyl]-4-fluorobenzenesulfonamide (25). 25** was obtained from **21a** (0.11 g, 0.5 mmol) and **14** (0.35 g, 0.5 mmol) as a yellow oil (0.19 g, 0.21 mmol, 42%). TLC (EA): R_f = 0.22. MS-ES-EM m/z = 929.2725 [(M + Na)$^+$] calcd for $C_{44}H_{47}FN_4O_{14}$Na 929.2697. HPLC t_R = 33.70 min (95.1%).

3-Benzo[1,3]dioxol-5-yl-4-{3-[2-(2-{2-[2-(4-fluoromethyl-1,2,3-triazol-1-yl)ethoxy]ethoxy}ethoxy)ethoxy]-4,5-dimethoxybenzyl}-5-hydroxy-5-(4-methoxyphenyl)-5*H*-furan-2-one (26). 26 was obtained from alkyne **22** and azide **14** (0.51 g, 0.74 mmol) as a yellow oil (0.16 g, 0.21 mmol, 28%). TLC (EA): R_f = 0.27. MS-ES-EM m/z = 774.2641 [(M + Na)$^+$] calcd for $C_{38}H_{42}FN_3O_{12}$-Na 774.2645. HPLC t_R = 22.28 min (96.0%).

Radiochemistry. General Methods. Radiofluorinations were carried out on a modified PET tracer radiosynthesizer (TRACERLab Fx_{FDG}, GE Healthcare). The recorded data were processed by the TRACERLab Fx software (GE Healthcare). No-carrier-added aqueous [^{18}F]fluoride was produced on a RDS 111e cyclotron (CTI-Siemens) by irradiation of a 1.2 mL water target using 10 MeV proton beams on 97.0% enriched ^{18}O-water by the ^{18}O(p,n)^{18}F nuclear reaction. Typical batches of [^{18}F]fluoride ions were 5.4−9.9 GBq at the end of radionuclide production for currents of 32 μA and irradiation times of 4 or 10 min, respectively. To recover the ^{18}O-water, the batch of aqueous [^{18}F]fluoride was passed through an anion exchange resin (Sep-Pak Light Waters Accell Plus QMA cartridge, preconditioned with 5 mL of 0.1 M $TBAHCO_3$ (pH 8.0) and 10 mL of water).

3-Benzo[1,3]dioxol-5-yl-4-{3-[1-(2-{2-[2-(2-[^{18}F]fluoroethoxy)-ethoxy]ethoxy}ethyl)-1*H*-1,2,3-triazol-4-ylmethoxy]-4,5-dimethoxybenzyl}-5-hydroxy-5-(4-methoxyphenyl)-5*H*-furan-2-one ([^{18}F]17). No-carrier-added [^{18}F]fluoride (5.4−9.9 GBq) was eluted from a QMA-cartridge with a solution of $TBAHCO_3$ (0.5 mL, 0.1 M, pH 8.0) and acetonitrile (0.5 mL). Subsequently, the aqueous [^{18}F]TBAF solution was carefully evaporated to dryness in vacuo. A solution of **27** (3.6 mg, 10 μmol) in anhydrous DMF (0.5 mL) was added and stirred for 10 min at 120 °C. The mixture was cooled to 60 °C, and a solution of **13** (7.8 mg, 15 μmol) in anhydrous DMF (0.2 mL), a solution of copper(II)sulfate pentahydrate (0.4 M, 120 μL), and a solution of sodium ascorbate (0.6 M, 240 μL) were added. After 10 min the mixture was diluted with a solution of 0.1 M K_2EDTA (13 mL) and passed through a Waters Sep-Pak Light C18 cartridge (preconditioned with 10 mL of ethanol and 10 mL of water). The cartridge was washed with 7 mL of water for injection, followed by elution of crude [^{18}F]**17** with 1.0 mL of acetonitrile (DNA-grade). An amount of 200 μL was fractionized by semipreparative HPLC procedure (conditions: λ = 254 nm; flow = 5.5 mL·min^{-1}; column = ACE-126-2510 (250 mm × 10 mm); 44% CH_3CN (0.1% TFA) in water (0.1% TFA) over 25 min). The solvent was evaporated in vacuo, and [^{18}F]**17** (~120 MBq) was formulated in saline/ethanol (10:1, 0.66 mL) for further experimental use. Starting from [^{18}F]fluoride the decay-corrected radiochemical yield of [^{18}F]**17** was 24 ± 9% (mean ± SD, decay-corrected, n = 3) after a total synthesis time of 130 min. Radiochemical purity (> 98%, t_R = 21.2 min) and specific radioactivity (17−35 GBq·μmol^{-1}) were determined by analytical radio-HPLC.

In Vitro Determination of Receptor Affinities. Microsomes were prepared by homogenizing myocardial ventricles from CD1 Nu/Nu mice at 4 °C for 90 s in 1 mL of buffer A (10 mM EDTA, 10 mM HEPES, 0.1 mM benzamidine, pH 7.4), using a Polytron PT 1200 (Kinematica, Lucerne, Switzerland). Homogenates were centrifuged at 45000g for 15 min at 4 °C. The pellets were resuspended in 1.8 mL of buffer B (1 mM EDTA, 10 mM HEPES, 0.1 mM benzamidine, pH 7.4) and recentrifuged at 45000g for 15 min at 4 °C. The pellets were resuspended in 1.8 mL of buffer B and centrifuged at 10000g for 10 min at 4 °C. The supernatants were recentrifuged at 45000g for 15 min at 4 °C. The pellets, partially enriched membranes, were resuspended in buffer C (50 mM Tris-HCl, 5 mM $MgCl_2$, pH 7.4) and stored frozen at −80 °C. For competition binding studies, the prepared membranes were resuspended in buffer D (10 mM Tris-HCl, 154 mM NaCl, 10 mM $MgCl_2$, 0.3% BSA pH 7.4) at 0 °C. An amount of 10 μg of membranes was incubated with constant concentrations of [^{125}I]ET-1 (40 pM, Perkin-Elmer Life Sciences Inc., Billerica, MA, U.S.) and with varying concentrations (1 pM to 10 μM) of ligands **17**, **19**, **23**−**26** at 37 °C for 2 h. Reactions were stopped by filtering onto Whatman GF/B filters and washed with distilled water. The membrane bound radioactivity was determined in a γ counter (Wallac Wizard). Competition binding curves were analyzed by nonlinear regression analysis using the XMGRACE program (Linux software). The high- and low-affinity IC_{50} values were converted into the high- and low-affinity inhibition constants ($K_i(ET_A)$and $K_i(ET_B)$) by the method of Cheng−Prusoff[57] using the previously determined K_D value of [^{125}I]ET-1.[58]

Determination of Partition Coefficient (log $D_{7.4}$). The lipophilicities of ^{18}F-labeled radioligands [^{18}F]**6** and [^{18}F]**17** were assessed by determination of the water−octanol partition coefficient by the following procedure.[59] 1-Octanol (0.5 mL) was added to a solution of approximately 20 kBq of the ^{18}F-labeled compound in PBS (0.5 mL, pH 7.4), and the layers were vigorously mixed for 1 min at room temperature. The tubes were centrifuged (3000 rpm, 2 min), and three samples of 100 μL of each layer were counted in a γ counter (Wallac Wizard). The partition coefficient was determined by calculating the ratio cpm(octanol)/cpm(PBS) and expressed as log $D_{7.4}$ (log($cpm_{octanol}$/cpm_{PBS})). Two independent experiments were performed in triplicate, and data were provided as mean values ± standard deviation.

Stability in Human Serum. The serum stabilities of ^{18}F-labeled compounds were evaluated by incubation in human serum at 37 °C for up to 120 min. An aliquot of the PBS-formulated ^{18}F-labeled compound (20 μL, 5 MBq) was added to a sample of human serum (200 μL), and the mixture was incubated at 37 °C. Samples of 20 μL each were taken after periods of 10, 20, 30, 60, 90, and 120 min and quenched in methanol/CH_2Cl_2 (1:1 v/v, 100 μL) followed by centrifugation for 2 min. The organic layer was analyzed by analytical radio-HPLC (flow, 1.5 mL·min^{-1}, linear gradient from 40% to 95% CH_3CN in water (0.1% TFA) over 5 min following 95% CH_3CN (0.1% TFA) in water (0.1% TFA) over 15 min, t_R = 17.2 min).

Ex Vivo Biodistribution Studies. Studies were carried out in mice, essentially as described previously.[35] Adult Balb/c mice (male and female, 25−32 g) were anesthetized by isoflurane/O_2, and fine catheters were inserted surgically into lateral tail veins. Animals were allowed to recover from the anesthesia for ~1 h, and during the studies they were conscious but under light restraint. [^{18}F]ET_A ligand [^{18}F]**17** (0.3−0.4 MBq, 2.5−2.7 nmol·g^{-1} body weight) was injected as a bolus (2 μL·g^{-1} body weight) via the tail vein 10 min after a bolus injection (1 μL·g^{-1} body weight) of **1** (sodium salt, dissolved in water) at 5 μmol·kg^{-1} (6 mice) or water for injection (five mice). Mice were killed by intravenous injection of sodium pentobarbitone (narcorin) at 200 mg·(kg body weight)$^{-1}$ and tissues were rapidly removed for measurement of radioactivity. In the first experiment (five mice) the first 2 cm of small intestine after the stomach (designated duodenum) was flushed with saline to remove its contents, cut open, and blotted dry. In the second experiment, the duodenum was cut open and its contents were removed to determine radioactivity. Radioactivity in each tissue was expressed as an uptake index, defined as

$$\text{uptake index} = \frac{\text{tissue radioactivity (cpm)/tissue wet weight (g)}}{\text{radioactivity injected (cpm)/body weight (g)}}$$

In Vivo PET Studies. Uptake of radioactivity after intravenous injection of ET_A receptor ligand [^{18}F]**17** was visualized using the high-resolution quadHIDAC small animal PET scanner (Oxford Positron Systems, Weston-on-the-Green, U.K.).[60] Balb/c mice (male and female, 22−25 g) were anesthetized with isoflurane (1.5%/0.3 L min^{-1}) and placed on a heating pad to maintain body temperature for insertion of tail vein catheters (26GA, BD VasculonPlus). For PET acquisition, animals were placed on a heat controlled multimodal scanning bed and PET list mode data were acquired for 90 min. The radioligand [^{18}F]**17** (5−10 MBq in 100 μL, 200 μL saline flush) was injected 30 s after the start of the acquisition. The scanner has an effective resolution

of 0.7 mm (fwhm) in the transaxial and axial directions when using an iterative resolution recovery reconstruction algorithm. Subsequently, the scanning bed was transferred to the computed tomography (CT) scanner (Inveon, Siemens Medical Solutions, U.S.) and a CT acquisition with a spatial resolution of 29 μm was performed for each mouse. Reconstructed image data sets were co-registered using extrinsic markers attached to the multimodal scanning bed and the image analysis software (Inveon Research Workplace 3.0, Siemens Medical Solutions, U.S.). On the basis of the CT data, three-dimensional volumes of interest (VOIs) were defined over the respective organs, transferred to the co-registered PET data, and analyzed quantitatively.

$$\%\ \mathrm{ID}\cdot\mathrm{mL}^{-1} = \frac{\text{radioactivity (cps)/mL in the VOI}}{\text{radioactivity (cps) mouse}} \times 100$$

Acknowledgment. The authors thank Anne Kanzog, Christine Bätza, Roman Priebe, and Claudia Gräf for technical support and the staff members of the Organic Chemistry Institute, University of Münster, Germany, for spectroscopic and analytical investigations. K.M. thanks Daniela Schrigten for synthesizing and providing compounds **18** and **27**. This study was supported by the Bundesministerium für Bildung und Forschung (BMBF), Germany (MoBiMed Subproject 01EZ0809), and the Deutsche Forschungsgemeinschaft (DFG), Germany (Grants SCHA 758/5-1 and SFB 656 A1/C6/Z5).

Supporting Information Available: Experimental procedures and analytical data for compounds **10a**, **10c**, **10d**, **12**, **13**, **15**, and **22** and ^{1}H, ^{13}C, and ^{19}F NMR data of compounds **19** and **23**−**26**. This material is available free of charge via the Internet at http://pubs.acs.org.

References

(1) Henry, P. J. Endothelin receptor distribution and function in the airways. *Clin. Exp. Pharamacol. Physiol.* **1999**, *26*, 162–167.
(2) Barton, M.; Yanagisawa, M. Endothelin: 20 years from discovery to therapy. *Can. J. Physiol. Pharmacol.* **2006**, *17*, 485–492.
(3) Dhaun, N.; Goddard, J.; Webb, D. J. The endothelin system and its antagonism in chronic kidney disease. *J. Am. Soc. Nephrol.* **2006**, *17*, 943–955.
(4) Giaid, A.; Yanagisawa, M.; Langleben, D.; Michel, R. P.; Levy, R.; Shennib, H.; Kimura, S.; Masaki, T.; Duguid, W. P.; Stewart, D. J. Expression of endothelin-1 in the lungs of patients with pulmonary hypertension. *N. Engl. J. Med.* **1993**, *328*, 1732–1739.
(5) Pittman, Q. J. Endothelin, an emerging role in proinflammatory pathways in brain. *Am. J. Physiol.: Regul. Integr. Comp. Physiol.* **2006**, *290*, R162–R163.
(6) Plusczyk, T.; Witzel, B.; Menger, M. D.; Schilling, M. ET_A and ET_B receptor function in pancreatitis-associated microcirculatory failure, inflammation, and parenchymal injury. *Am. J. Physiol.: Gastrointest. Liver Physiol.* **2003**, *285*, G145–G153.
(7) Saito, Y.; Nakao, K.; Mukoyama, M.; Imura, H. Increased plasma endothelin level in patients with essential hypertension. *N. Engl. J. Med.* **1990**, *322*, 205.
(8) Teerlink, J. R.; Loffler, B. M.; Hess, P.; Maire, J. P.; Clozel, M.; Clozel, J. P. Role of endothelin in the maintenance of blood pressure in conscious rats with chronic heart failure. Acute effects of the endothelin receptor antagonist Ro 47-0203 (bosentan). *Circulation* **1994**, *90*, 2510–2518.
(9) Nelson, J.; Bagnato, A.; Battistini, B.; Nisen, P. The endothelin axis: emerging role in cancer. *Nat. Rev. Cancer* **2003**, *3*, 110–116.
(10) Bagnato, A.; Natali, P. G. Targeting endothelin axis in cancer. *Cancer Treat. Res.* **2004**, *119*, 293–314.
(11) Bagnato, A.; Rosanò, L. The endothelin axis in cancer. *Int. J. Biochem. Cell Biol.* **2008**, *40*, 1443–1451.
(12) Bagnato, A.; Spinella, F.; Rosanò, L. The endothelin axis in cancer: the promise and the challenges of molecularly targeted therapy. *Can. J. Physiol. Pharmacol.* **2008**, *86*, 473–484.
(13) Asham, E.; Shankar, A.; Loizidou, M.; Fredericks, S.; Miller, K.; Boulos, P. B.; Burnstock, G.; Taylor, I. Increased endothelin-1 in colorectal cancer and reduction of tumour growth by ET(A) receptor antagonism. *Br. J. Cancer* **2001**, *85*, 1759–1763.
(14) Bagnato, A.; Salani, D.; Di Castro, V.; Wu-Wong, J. R.; Tecce, R.; Nicotra, M. R.; Venuti, A.; Natali, P. G. Expression of endothelin 1 and endothelin A receptor in ovarian carcinoma: evidence for an autocrine role in tumor growth. *Cancer Res.* **1999**, *59*, 720–727.
(15) Nelson, J. B.; Chan-Tack, K.; Hedican, S. P.; Magnuson, S. R.; Opgenorth, T. J.; Bova, G. S.; Simons, J. W. Endothelin-1 production and decreased endothelin B receptor expression in advanced prostate cancer. *Cancer Res.* **1996**, *56*, 663–668.
(16) Alanen, K.; Deng, D. X.; Chakrabarti, S. Augmented expression of endothelin-1, endothelin-3 and the endothelin-B receptor in breast carcinoma. *Histopathology* **2000**, *36*, 161–167.
(17) Wülfing, P.; Diallo, R.; Kersting, C.; Wülfing, C.; Poremba, C.; Rody, A.; Greb, R. R.; Boecker, W.; Kiesel, L. Expression of endothelin-1, endothelin-A, and endothelin-B receptor in human breast cancer and correlation with long-term follow-up. *Clin. Cancer Res.* **2003**, *9*, 4125–4131.
(18) Rosano, L.; Varmi, M.; Salani, D.; Di Castro, V.; Spinella, F.; Natali, P. G.; Bagnato, A. Endothelin-1 induces tumor proteinase activation and invasiveness of ovarian carcinoma cells. *Cancer Res.* **2001**, *61*, 8340–8346.
(19) Salani, D.; Di Castro, V.; Nicotra, M. R.; Rosano, L.; Tecce, R.; Venuti, A.; Natali, P. G.; Bagnato, A. Role of endothelin-1 in neovascularization of ovarian carcinoma. *Am. J. Pathol.* **2000**, *157*, 1537–1547.
(20) Del Bufalo, D.; Di Castro, V.; Biroccio, A.; Varmi, M.; Salani, D.; Rosano, L.; Trisciuoglio, D.; Spinella, F.; Bagnato, A. Endothelin-1 protects ovarian carcinoma cells against paclitaxel induced apoptosis: requirement for Akt activation. *Mol. Pharmacol.* **2002**, *61*, 524–532.
(21) Eberl, L. P.; Egidy, G.; Pinet, F.; Juillerat-Jeanneret, L. Endothelin receptor blockade potentiates FasL-induced apoptosis in colon carcinoma cells via the protein kinase C-pathway. *J. Cardiovasc. Pharmacol.* **2000**, *36*, S354–356.
(22) Ali, H.; Dashwood, M.; Dawas, K.; Loizidou, M.; Savage, F.; Taylor, I. Endothelin receptor expression in colorectal cancer. *J. Cardiovasc. Pharmacol.* **2000**, *36*, S69–71.
(23) Winn, M.; Boyd, S. A.; Hutchins, C. W.; Jae, H.-S.; Tasker, A. S.; Vongeldern, T. W.; Kester, J. A.; Sorensen, B. K. Preparation of Pyrrolidinecarboxylic Acid Derivatives and Analogs as Endothelin Antagonists. WO 9606095 A1 19960229, Feb 29, 1996; Abbott Laboratories, U.S.
(24) Bagnato, A.; Cirilli, A.; Salani, D.; Simeone, P.; Muller, A.; Nicotra, M. R.; Natali, P. G.; Venuti, A. Growth inhibition of cervix carcinoma cells in vivo by endothelin A receptor blockade. *Cancer Res.* **2002**, *62*, 6381–6384.
(25) Rosano, L.; Spinella, F.; Salani, D.; Di Castro, V.; Venuti, A.; Nicotra, M. R.; Natali, P. G.; Bagnato, A. Therapeutic targeting of the endothelin A receptor in human ovarian carcinoma. *Cancer Res.* **2003**, *63*, 2447–2453.
(26) Carducci, M. A.; Nelson, J. B.; Bowling, M. K.; Rogers, T.; Eisenberger, M. A.; Sinibaldi, V.; Donehower, R.; Leahy, T. L.; Carr, R. A.; Isaacson, J. D.; Janus, T. J.; Andre, A.; Hosmane, B. S.; Padley, R. J. Atrasentan, an endothelin-receptor antagonist for refractory adenocarcinomas: safety and pharmacokinetics. *J. Clin. Oncol.* **2002**, *20*, 2171–2180.
(27) Carducci, M. A.; Padley, R. J.; Breul, J.; Vogelzang, N. J.; Zonnenberg, B. A.; Daliani, D. D.; Schulman, C. C.; Nabulsi, A. A.; Humerickhouse, R. A.; Weinberg, M. A.; Schmitt, J. L.; Nelson, J. B. Effect of endothelin-A receptor blockade with atrasentan on tumor progression in men with hormone-refractory prostate cancer: a randomized, phase II, placebo-controlled trial. *J. Clin. Oncol.* **2003**, *21*, 679–689.
(28) Mathews, W. B.; Zober, T. G.; Ravert, H. T.; Scheffel, U.; Hilton, J.; Sleep, D.; Dannals, R. F.; Szabo, Z. Synthesis and in vivo evaluation of a PET radioligand for imaging the endothelin-A receptor. *Nucl. Med. Biol.* **2006**, *33*, 15–19.
(29) Aleksic, S.; Szabo, Z.; Scheffel, U.; Ravert, H. T.; Mathews, W. B.; Kerenyi, L.; Rauseo, P. A.; Gibson, R. E.; Burns, H. D.; Dannals, R. F. In vivo labeling of endothelin receptors with [(11)C]L-753,037: studies in mice and a dog. *J. Nucl. Med.* **2001**, *42*, 1274–1280.
(30) Johnstrøm, P.; Fryer, T. D.; Richards, H. K.; Barret, O.; Clark, J. C.; Ohlstein, E. H.; Pickard, J. D.; Davenport, A. P. In vivo imaging of cardiovascular endothelin receptors using the novel radiolabelled antagonist [^{18}F]-SB209670 and positron emission tomography (microPET). *J. Cardiovasc. Pharmacol.* **2004**, *44*, S34–S38.
(31) Berryman, K. A.; Doherty, A. M.; Edmunds, J. J.; Patt, W. C.; Plummer, M. S.; Repine, J. T. Preparation of 2(5*H*)-Furanones, 2(5*H*)-Thiophenones, 2(5*H*)-Pyrrolones and Benzodioxolyls as Endothelin Antagonists. WO 9505376 A1 19950223, Feb 23, 1995; Warner Lambert Co., U.S.
(32) Doherty, A. M.; Patt, W. C.; Edmunds, J. J.; Berryman, K. A.; Reisdorph, B. R.; Plummer, M. S.; Shahripour, A.; Lee, C.; Cheng,

X. M.; Walker, D. M. Discovery of a novel series of orally active non-peptide endothelin-A (ET_A) receptor-selective antagonists. *J. Med. Chem.* **1995**, *38*, 1259–1263.
(33) Patt, W. C.; Edmunds, J. J.; Repine, J. T.; Berryman, K. A.; Reisdorph, B. R.; Lee, C.; Plummer, M. S.; Shahripour, A.; Haleen, S. J.; Keiser, J. A.; Flynn, M. A.; Welch, K. M.; Reynolds, E. E.; Rubin, R.; Tobias, B.; Hallak, H.; Doherty, A. M. J. Structure−activity relationships in a series of orally active gamma-hydroxy butenolide endothelin antagonists. *J. Med. Chem.* **1997**, *40*, 1063–1074.
(34) Höltke, C.; von Wallbrunn, A.; Kopka, K.; Schober, O.; Heindel, W.; Schäfers, M.; Bremer, C. A fluorescent photoprobe for the imaging of endothelin receptors. *Bioconjugate Chem.* **2007**, *18*, 685–694.
(35) Höltke, C.; Law, M. P.; Wagner, S.; Kopka, K.; Faust, A.; Breyholz, H. J.; Schober, O.; Bremer, C.; Riemann, B.; Schäfers, M. PET-compatible endothelin receptor radioligands: synthesis and first in vitro and in vivo studies. *Bioorg. Med. Chem.* **2009**, *17*, 7197–7208.
(36) Kuc, R. E.; Maguire, J. J.; Davenport, A. P. Quantification of endothelin receptor subtypes in peripheral tissues reveals down-regulation of ET_A receptors in ET_B-deficient mice. *Exp. Biol. Med.* **2006**, *231*, 741–745.
(37) Hamidi, M.; Azadi, A.; Rafiei, P. Pharmacokinetic consequences of pegylation. *Drug Delivery* **2006**, *13*, 399–409.
(38) Harris, J. M.; Chess, R. B. Effect of pegylation on pharmaceuticals. *Nat. Rev. Drug Discovery* **2003**, *2*, 214–221.
(39) Greenwald, R. B.; Choe, Y. H.; McGuire, J.; Conover, C. D. Effective drug delivery by PEGylated drug conjugates. *Adv. Drug Delivery Rev.* **2003**, *55*, 217–250.
(40) Kolb, H. C.; Sharpless, K. B. The growing impact of click chemistry on drug discovery. *Drug Discovery Today* **2003**, *8*, 1128–1137.
(41) Manetsch, R.; Krasinnski, A.; Radic, Z.; Raushel, J.; Taylor, P.; Sharpless, K. B.; Kolb, H. C. In situ click chemistry: enzyme inhibitors made to their own specifications. *J. Am. Chem. Soc.* **2004**, *126*, 12809–12818.
(42) Kolb, H. C.; Finn, M. G.; Sharpless, K. B. Click-chemie: diverse chemische Funktionalität mit einer handvoll guter reaktionen. *Angew. Chem.* **2001**, *113*, 2056–2075; Click chemistry: diverse chemical function from a few good reactions *Angew. Chem., Int. Ed.* **2001**, *40*, 2004−2021 .
(43) Breyholz, H. J.; Wagner, S.; Faust, A.; Riemann, B.; Höltke, C.; Hermann, S.; Schober, O.; Schäfers, M.; Kopka, K. Radiofluorinated pyrimidine-2,4,6-triones as molecular probes for noninvasive MMP-targeted imaging. *ChemMedChem* **2010**, *5*, 777–789.
(44) Marik, J.; Sutcliffe, J. L. Click for PET: rapid preparation of [^{18}F]fluoropeptides using Cu^{I} catalyzed 1,3-dipolar cycloaddition. *Tetrahedron Lett.* **2006**, *47*, 6681–6684.
(45) Glaser, M.; Arstad, E. "Click labeling" with 2-[^{18}F]fluoroethylazide for positron emission tomography. *Bioconjugate Chem.* **2007**, *18*, 989–993.
(46) Li, Z.-B.; Wu, Z.; Chen, K.; Chin, F. T.; Chen, X. Click chemistry for ^{18}F-labeling of RGD peptides and microPET imaging of tumor integrin $\alpha_v\beta_3$ expression. *Bioconjugate Chem.* **2007**, *18*, 1987–1994.
(47) Ramenda, T.; Bergmann, R.; Wuest, F. Synthesis of ^{18}F-labeled neurotensin(8−13) via copper-mediated 1,3-dipolar [3+2]cycloaddition reaction. *Lett. Drug Des. Discovery* **2007**, *4*, 279–285.
(48) Ross, T. L.; Honer, M.; Lam, P. Y.; Mindt, T. L.; Groehn, V.; Schibli, R.; Schubiger, P. A.; Ametamey, S. M. Fluorine-18 click radiosynthesis and preclinical evaluation of a new ^{18}F-labeled folic acid derivative. *Bioconjugate Chem.* **2008**, *19*, 2462–2470.
(49) Thonon, D.; Kech, C.; Paris, J.; Lemaire, C.; Luxen, A. New strategy for the preparation of clickable peptides and labeling with 1-(azidomethyl)-4-[^{18}F]-fluorobenzene for PET. *Bioconjugate Chem.* **2009**, *20*, 817–823.
(50) Maschauer, S.; Einsiedel, J.; Haubner, R.; Hocke, C.; Ocker, M.; Hübner, H.; Kuwert, T.; Gmeiner, P.; Prante, O. Markierung und glycosylierung von peptiden mithilfe der klick-chemie: ein allgemeiner ansatz zur synthese von ^{18}F-glycopeptiden, leistungsstarken tracern für die positronenemissionstomographie. *Angew. Chem.* **2010**, *122*, 988–992; Labeling and glycosylation of peptides using click chemistry: a general approach to ^{18}F-glycopeptides as effective imaging probes for positron emission tomography *Angew. Chem., Int. Ed.* **2010**, *49*, 976−979 .
(51) Zoghbi, S. S.; Shetty, H. U.; Ichise, M.; Fujita, M.; Imaizumi, M.; Liow, J.-S.; Shah, J.; Musachio, J. L.; Pike, V. W.; Innis, R. B. PET imaging of the dopamine transporter with ^{18}F-FECNT: a polar radiometabolite confounds brain radioligand measurements. *J. Nucl. Med.* **2006**, *47*, 520–527.
(52) Ramenda, T.; Kniess, T.; Bergmann, R.; Steinbach, J.; Wuest, F. Radiolabelling of proteins with fluorine-18 via click chemistry. *Chem. Commun.* **2009**, *48*, 7521–7523.
(53) Inkster, J. A. H.; Guérin, B.; Ruth, T. J.; Adam, M. J. Radiosynthesis and bioconjugation of [^{18}F]FPy5yne, a prosthetic group for the ^{18}F labeling of bioactive peptides. *J. Labelled Compd. Radiopharm.* **2008**, *51*, 444–452.
(54) Zhu, L.; Liu, J. Fluorine-Containing Tetrabenazine Derivative as Vesicular Monoamine Transporter-Targeted Agent and Its Preparation Method. CN 101537193, A 20090923, Sept 23, 2009; Beijing Normal University, P. R. China.
(55) Schrigten, D. Ph.D. Thesis, University of Münster, Münster, Germany. Unpublished results.
(56) Kuhnast, B.; Damont, A.; Hinnen, F.; Huss, C.; Dollé, F. PEG-[^{18}F]FPyZIDE and PEG-[^{18}F]FPyKYNE, two new fluoropyridine-based reagents for the fluorine-18 labeling of macromolecules using click chemistry. *J. Labelled Compd. Radiopharm.* **2009**, *52* (S1), S184.
(57) Cheng, Y.; Prusoff, W. H. Relationship between the inhibition constant (K1) and the concentration of inhibitor which causes 50 per cent inhibition (I50) of an enzymatic reaction. *Biochem. Pharmacol.* **1973**, *22*, 3099–3108.
(58) Höltke, C.; Law, M. P.; Wagner, S.; Breyholz, H. J.; Kopka, K.; Bremer, C.; Levkau, B.; Schober, O.; Schäfers, M. Synthesis, in vitro pharmacology and biodistribution studies of new PD 156707-derived ET_A receptor radioligands. *Bioorg. Med. Chem.* **2006**, *14*, 1910–1917.
(59) Prante, O.; Hocke, C.; Löber, S.; Hübner, H.; Gmeiner, P.; Kuwert, T. Tissue distribution of radioiodinated FAUC113: assessment of a pyrazolo(1,5-*a*)pyridine based dopamine D4 receptor radioligand candidate. *Nuklearmedizin* **2006**, *45*, 41–44.
(60) Schäfers, K. P.; Reader, A. J.; Kriens, M.; Knoess, C.; Schober, O.; Schäfers, M. Performance evaluation of the 32-module quad-HIDAC small-animal PET scanner. *J. Nucl. Med.* **2005**, *46*, 996–1004.